

Probes of the small x gluon via exclusive J/ψ and Υ production at HERA and the LHC

S.P. JONES^a, A.D. MARTIN^b, M.G. RYSKIN^{b,c} and T. TEUBNER^a

^a *Department of Mathematical Sciences,
University of Liverpool, Liverpool L69 3BX, U.K.*

^b *Department of Physics and Institute for Particle Physics Phenomenology,
University of Durham, Durham DH1 3LE, U.K.*

^c *Petersburg Nuclear Physics Institute, NRC Kurchatov Institute, Gatchina, St. Petersburg,
188300, Russia*

Abstract

New, more precise data on diffractive J/ψ photoproduction and on exclusive J/ψ production in the process $pp \rightarrow p + J/\psi + p$ at the LHC allow a better constraint on the low- x gluon distribution in the domain of relatively low scales $Q^2 \sim 2 - 6 \text{ GeV}^2$. We account for the ‘skewed’ effect and for the real part of the amplitude, as well as for the absorptive corrections in the case of the exclusive process $pp \rightarrow p + J/\psi + p$. The predictions for exclusive J/ψ production at $\sqrt{s} = 8$ and 14 TeV and for exclusive $\Upsilon(1S)$ production at 7, 8 and 14 TeV are also given. We present results at leading and next-to-leading order.

1 Introduction

The low x behaviour of the gluon parton distribution function (PDF) is still not well established by the current global parton analyses. At next-to-leading order (NLO) the difference

between the gluon PDF found in the analyses of the different groups is relatively large, and the uncertainty corridors are big, especially at relatively low scales, $Q^2 \sim 2 - 6 \text{ GeV}^2$. On the other hand, diffractive vector meson (J/ψ , Υ) production, for which the cross section is proportional to the *square* of the gluon distribution, provides important additional information in just this kinematic region. At the moment, these data have not been included in the global parton analyses, since (a) strictly speaking the cross section is proportional to the generalised gluon PDF and not the usual diagonal PDF, and, (b) there are some problems in implementing the NLO coefficient function¹ corresponding to this process.

The first problem may be solved in the low x region using the Shuvaev transform [2], which facilitates the relation between the generalised and diagonal PDFs to an accuracy of $\mathcal{O}(x)$. Coming to the second problem, we approximate the NLO corrections to the coefficient function by accounting for the explicit k_T integration in the last step of the interaction. This is not the complete NLO contribution, but in this way we are able to include the most important NLO effect.

The corresponding analysis was performed in 2008, and described in detail in [3]. However new and more precise data have been published by the HERA experiment H1 [4], and in addition the LHCb collaboration have recently presented data on exclusive (ultraperipheral) J/ψ production [5] which is sensitive to, and enlarges, the low x interval. These $pp \rightarrow p + J/\psi + p$ data enable us to improve the determination of the gluon, but require an extension of the theoretical framework and necessitate the inclusion of absorptive corrections.

2 Exclusive J/ψ production at HERA

We recall the lowest order Feynman diagram for the cross section for the process $\gamma^*p \rightarrow J/\psi p$, shown in Fig. 1. The corresponding expression for the cross section in leading logarithmic (LO) approximation using the non-relativistic approximation for the J/ψ meson is [6]

$$\frac{d\sigma}{dt} (\gamma^*p \rightarrow J/\psi p) \Big|_{t=0} = \frac{\Gamma_{ee} M_{J/\psi}^3 \pi^3}{48\alpha} \left[\frac{\alpha_s(\bar{Q}^2)}{\bar{Q}^4} xg(x, \bar{Q}^2) \right]^2 \left(1 + \frac{Q^2}{M_{J/\psi}^2} \right). \quad (1)$$

Here Γ_{ee} is the electronic width of the J/ψ , and

$$\bar{Q}^2 = (Q^2 + M_{J/\psi}^2)/4, \quad x = (Q^2 + M_{J/\psi}^2)/(W^2 + Q^2). \quad (2)$$

Q^2 is the virtuality of the photon, $M_{J/\psi}$ is the rest mass of the J/ψ , and W is the γ^*p centre-of-mass energy. Equation (1) gives the differential cross section at zero momentum transfer, $t = 0$. To describe data integrated over t , the integration is carried out assuming $\sigma \sim \exp(-Bt)$ with B the experimentally measured slope parameter. For J/ψ we use the W dependent slope

$$B(W) = (4.9 + 4\alpha' \ln(W/W_0)) \text{ GeV}^{-2}, \quad (3)$$

¹Progress is underway to illuminate certain aspects of the existing NLO calculation [1], and to fix an optimal factorisation scale sampled by this process $\gamma^*p \rightarrow Vp$.

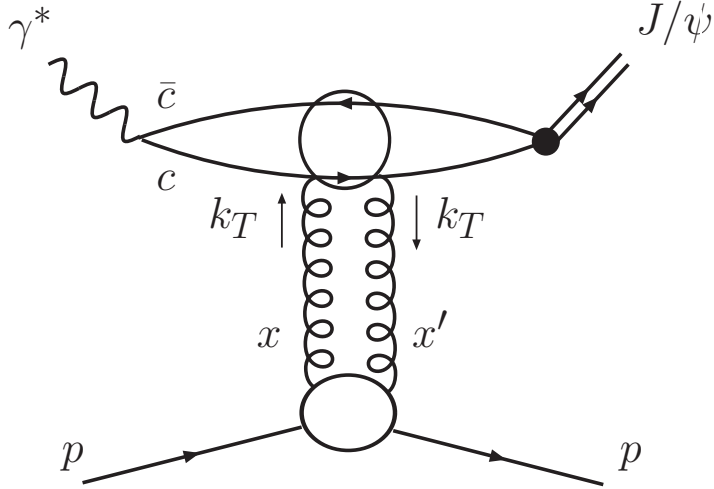


Figure 1: Schematic picture of high energy exclusive J/ψ production, $\gamma^* p \rightarrow J/\psi p$. The factorised form follows since, in the proton rest frame, the formation time $\tau_f \simeq 2E_\gamma/(Q^2 + M_{J/\psi}^2)$ is much greater than the $c\bar{c}$ -proton interaction time τ_{int} . In the case of the simple two-gluon exchange shown here, $\tau_{\text{int}} \simeq R_p$, where R_p is the radius of the proton.

where $\alpha' = 0.06$ and $W_0 = 90$ GeV. This slope grows more slowly with W than the formula used by H1 [7], but is compatible with the HERA data and with the slope and α' of model 4 of [8] used below in Section 3 to calculate the gap survival probability S^2 in the case of $pp \rightarrow p + J/\psi + p$ process measured by LHCb.

Thus it becomes possible, in principle, to extract the gluon density $xg(x, \bar{Q}^2)$ directly from the measured diffractive J/ψ cross section. However, first, let us list the corrections to the leading order expression. Expression (1) is a simple first approximation, justified in the leading order (LO) collinear approximation using the non-relativistic J/ψ wave function. It was shown by Hoodbhoy [9] that the relativistic corrections to (1), written in terms of the experimentally measured Γ_{ee} , are small, $\sim \mathcal{O}(4\%)$, and we neglect them.

We also need to account for the fact that the two exchanged gluons carry different fractions x, x' of the light-cone proton momentum, see Fig. 1. That is, we have to use the generalised (skewed) gluon distribution. In our case $x' \ll x \ll 1$, and the skewing effect can be well estimated from [2] – the amplitude should be multiplied by

$$R_g = \frac{2^{2\lambda+3} \Gamma(\lambda + \frac{5}{2})}{\sqrt{\pi} \Gamma(\lambda + 4)}, \quad (4)$$

where $\lambda(Q^2) = \partial [\ln(xg)] / \partial \ln(1/x)$ (for a more detailed discussion see [10]). In other words, in the small x region of interest, we take the gluon to have the form $xg \sim x^{-\lambda}$, where λ may be scale dependent.

The diagonal PDF corresponds to the discontinuity (i.e. the imaginary part) of the amplitude shown in Fig. 1. The real part may be determined using a dispersion relation. In the low x region, for our positive-signature amplitude $A \propto x^{-\lambda} + (-x)^{-\lambda}$, the dispersion relation gives

$$\frac{\text{Re}A}{\text{Im}A} \simeq \frac{\pi}{2}\lambda \simeq \frac{\pi}{2} \frac{\partial \ln A}{\partial \ln(1/x)} \simeq \frac{\pi}{2} \frac{\partial \ln(xg(x, \bar{Q}^2))}{\partial \ln(1/x)}. \quad (5)$$

To mimic the main effect of the NLO corrections to the coefficient function (upper part in Fig. 1), we perform an explicit k_T^2 integration in the last step of the evolution. We thus introduce the unintegrated gluon distribution, $f(x, k_T^2)$, which is related to the integrated gluon by

$$xg(x, \mu^2) = \int_{Q_0^2}^{\mu^2} \frac{dk_T^2}{k_T^2} f(x, k_T^2) + c(Q_0^2). \quad (6)$$

Strictly speaking we have to include in f the Sudakov factor $T(k^2, \mu^2)$ to account for the fact that no additional gluons with transverse momentum larger than k_T are emitted, where

$$T(k_T^2, \mu^2) = \exp \left[\frac{-C_A \alpha_s(\mu^2)}{4\pi} \ln^2 \left(\frac{\mu^2}{k_T^2} \right) \right] \quad (7)$$

and $T = 1$ for $k_T^2 \geq \mu^2$, such that [11, 12]

$$f(x, k_T^2) = \partial [xg(x, k_T^2)T(k_T^2, \mu^2)] / \partial \ln k_T^2. \quad (8)$$

Moreover for skewed distributions with $x' \ll x$ only the hard parton with momentum fraction x may emit bremsstrahlung gluons (the parton with x' is too slow). Therefore our unintegrated *skewed* distribution should be replaced by

$$f(x, x', k_T^2, \mu^2) = \partial \left[xg(x, k_T^2) \sqrt{T(k_T^2, \mu^2)} \right] / \partial \ln k_T^2, \quad (9)$$

and the scale $\mu = \max(k_T^2, \bar{Q}^2)$ is chosen. Numerically the correction from the inclusion of the Sudakov factor is negligible. The dominant contribution comes from the region of $k_T \sim \bar{Q}$ where $T(k_T^2, \mu^2)$ is close to unity with the natural scale choice $\mu^2 = \bar{Q}^2$. The inclusion of the T factor may be considered as an $\mathcal{O}(\alpha_s)$ correction to the gluon density; it affects the gluon in our analysis only marginally. For example, it enhances the gluon by about 0.5% for the photoproduction scale $\bar{Q}^2 = 2.4 \text{ GeV}^2$ and $x = 10^{-3}$.

For the infra-red region of $k_T < Q_0$ we assume a linear behaviour of $xg(x, k_T^2) \sqrt{T(k_T^2, \mu^2)}$ at small k_T^2 , giving

$$xg(x, k_T^2) \sqrt{T(k_T^2, \mu^2)} = xg(x, Q_0^2) \sqrt{T(Q_0^2, \mu_{\text{IR}}^2)} k_T^2 / Q_0^2. \quad (10)$$

The scale of α_s in the infra-red contribution is chosen as $\mu_{\text{IR}}^2 = \max(Q_0^2, \bar{Q}^2)$ which matches the lowest scales of α_s sampled in the k_T^2 integral.

The net result of the changes is that in (1) we have to make the replacement

$$\left[\frac{\alpha_s(\bar{Q}^2)}{\bar{Q}^4} xg(x, \bar{Q}^2) \right] \longrightarrow \int_{Q_0^2}^{(W^2 - M_{J/\psi}^2)/4} \frac{dk_T^2 \alpha_s(\mu^2)}{\bar{Q}^2(\bar{Q}^2 + k_T^2)} \frac{\partial \left[xg(x, k_T^2) \sqrt{T(k_T^2, \mu^2)} \right]}{\partial k_T^2} + \ln \left(\frac{\bar{Q}^2 + Q_0^2}{\bar{Q}^2} \right) \frac{\alpha_s(\mu_{IR}^2)}{\bar{Q}^2 Q_0^2} xg(x, Q_0^2) \sqrt{T(Q_0^2, \mu_{IR}^2)}. \quad (11)$$

[The original LO result (1) was obtained by integrating the factor $\alpha_s f(x, k_T^2)/(\bar{Q}^2 + k_T^2)$ in the amplitude over dk_T^2/k_T^2 , and keeping just the leading logarithmic result, $\alpha_s(\bar{Q}^2)xg(x, \bar{Q}^2)/\bar{Q}^2$.]

For the LO and NLO descriptions we use a one-loop and two-loop running α_s , respectively, with $\alpha_s(M_Z^2) = 0.118$ and heavy quarks decoupled at the scale m_Q , with m_Q the heavy quark mass in the on-shell scheme [13].

3 Ultraperipheral production at the LHC

In this Section we consider the process $pp \rightarrow p + J/\psi + p$. At the moment the LHC experiments are unable to tag forward protons accompanying the J/ψ . Instead the exclusivity is provided by selecting events with large rapidity gaps on both sides of the J/ψ and fitting the p_T distribution of the J/ψ with two components: one with a small p_T and one with a large p_T . It is assumed that the small p_T component corresponds to the exclusive process [5]. Indeed, the exclusive production amplitude is described by the sum of the two diagrams shown in Fig. 2. In this configuration the momentum transverse to the J/ψ is limited by the proton form factors. If one or two protons dissociate, then the typical transverse momentum of the J/ψ will be much larger.

Photon exchange may be replaced by odderon exchange [14], however, even if it is not negligible, the odderon contribution will also occur in a larger p_T region. Thus the selection of the small p_T component will provide sufficient exclusivity of the process.

For exclusive J/ψ production in pp collisions we have to include absorptive corrections. For production at HERA, the absorptive corrections are expected to be smaller. The transverse size, r , of the $q\bar{q}$ dipole produced by the ‘heavy’ photon in deep inelastic scattering has a logarithmic distribution $\int dr^2/r^2$ starting from $1/Q^2$ up to some hadronic scale. In the case of J/ψ production the size of the $c\bar{c}$ dipole is limited by the size of the J/ψ meson. Even in photoproduction it is of the order of $1/\bar{Q}^2$. Since the probability of rescattering is proportional to r^2 , we anticipate a much smaller absorptive effect.

On the contrary, at the LHC, there is a probability of an additional soft interaction between the two colliding protons which will generate secondaries that will populate the rapidity gaps used to select an exclusive event. Therefore, to include the LHCb J/ψ data in the fit, we must first allow for the gap survival effect. These absorptive corrections are calculated using

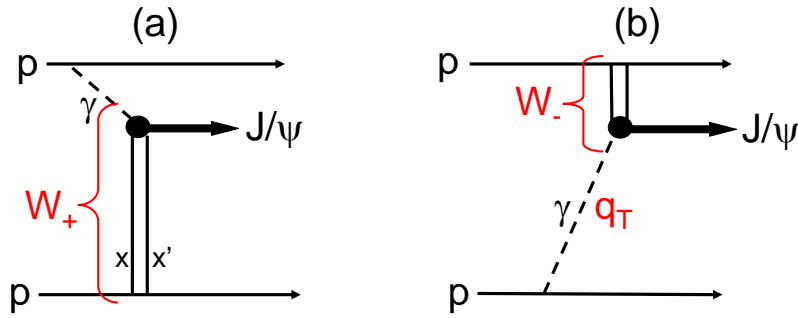


Figure 2: The two diagrams describing exclusive J/ψ production at the LHC. The vertical lines represent two-gluon exchange. Diagram (a), the W_+ component, is the major contribution to the $pp \rightarrow p + J/\psi + p$ cross section for a J/ψ produced at large rapidity y . Thus such data allow a probe of very low x values, $x \sim M_{J/\psi} \exp(-y)/\sqrt{s}$; recall that for two-gluon exchange we have $x \gg x'$.

an eikonal model. It is convenient to work in the impact parameter (b_t) representation, where the suppression factor for the cross section is

$$S^2 = \langle s^2(b_t) \rangle = \frac{\int \sum_i |\mathcal{M}_i(s, b_t^2)|^2 \exp[-\Omega_i(s, b_t^2)] d^2b_t}{\int \sum_i |\mathcal{M}_i(s, b_t^2)|^2 d^2b_t}, \quad (12)$$

with $\mathcal{M}_i(s, b_t^2)$ the diffractive amplitudes in impact parameter space and $\Omega_i(b_t)$ the proton opacities, see [15] for details.

In order to extract the $\gamma^*p \rightarrow J/\psi p$ cross section, the LHCb collaboration have used the absorptive factors calculated in Ref. [16] based on a one-channel eikonal model. The corresponding suppression factor is not strong (typically $S^2 \sim 0.8$) since photon exchange mainly occurs at relatively large values of b_t , where the proton opacity $\Omega(b_t)$ is already small. Indeed, the photon flux dn/dk is given by the integral over the photon q_T which has a logarithmic form,

$$\frac{dn}{dk} = \frac{\alpha}{\pi k} \int_0^\infty dq_T^2 \frac{q_T^2 F_p^2(q_T^2)}{(t_{\min} + q_T^2)^2}, \quad \text{where} \quad t_{\min} \simeq \frac{(x_\gamma m_p)^2}{1 - x_\gamma}, \quad (13)$$

with $k = x_\gamma \sqrt{s}/2$ and x_γ the momentum fraction of the emitting proton carried by the photon. In the integral q_T^2 effectively runs from t_{\min} to $1/R_p^2$, where R_p is the proton radius. At the upper end, the integral is limited by the proton form factor, F_p . At the lower end of integration, with LHC kinematics, the value of t_{\min} is quite small; the corresponding photon momentum fractions x_γ^\pm are

$$x_\gamma^\pm = \frac{M_{J/\psi}}{\sqrt{s}} e^{\pm y}, \quad \text{giving} \quad t_{\min} \simeq \frac{m_p^2 M_{J/\psi}^2}{s} e^{\pm 2y}, \quad (14)$$

where y is the rapidity of the J/ψ . Thus the typical b_t values are quite large, of the order of $\sqrt{s}/(m_p M_{J/\psi})$. Only the upper end of the q_T integral, where $b_t \sim R_p$, is affected by absorptive corrections.

A deficiency of the LHCb extraction of the $\gamma^*p \rightarrow J/\psi p$ cross section from their data is that the same survival factor, $r(y)$, was used for both diagrams of Fig. 2(a) and (b), whereas, at non-zero rapidity, y , the value of t_{\min} , and the corresponding value of b_t , are quite different for large ($W_+^2 = M_{J/\psi}\sqrt{s}e^y$) and small ($W_-^2 = M_{J/\psi}\sqrt{s}e^{-y}$) photon-proton centre-of-mass energies squared.

In the present analysis we fit to LHCb measurements of $d\sigma(pp \rightarrow p + J/\psi + p)/dy$ using the proton form factor given by

$$F_p(q_T^2) = \left(1 + \frac{t_{\min} + q_T^2}{0.71 \text{ GeV}^2}\right)^{-2}, \quad (15)$$

and survival factors calculated from a two-channel eikonal model [8]. This model had been previously obtained by fitting to the TOTEM data [17] for elastic pp scattering, $d\sigma_{\text{el}}/dt$, and to the TOTEM estimate for low-mass diffractive dissociation at 7 TeV, as well as the ATLAS data for $d\sigma/d\Delta\eta$ which constrain high-mass diffractive dissociation. Thus, in our calculation of $d\sigma(pp \rightarrow p + J/\psi + p)/dy$, we include both diagrams (a) and (b), each with their corresponding absorptive corrections.

We account for the transverse polarisation of the J/ψ in the $\gamma p \rightarrow J/\psi p$ amplitude, A , as described in [15]. The vector structure of the amplitude is important since it leads to the vanishing of the amplitude $A \propto b_t$ in the centre of the impact parameter space ($b_t \rightarrow 0$), precisely in the region where the suppression (12) is especially strong.

For completeness, we list, in Tables 2 and 3 respectively, the survival factors relevant to exclusive J/ψ and $\Upsilon(1S)$ production at LHCb. The rapidity range covered by ATLAS and CMS corresponds to a smaller $|y|$. Therefore the energies W_{\pm} probed by these experiments are similar to that of HERA.

Contrary to the pp case, in heavy ion (Pb-Pb) collisions the dominant contribution comes from the W_- amplitude since for the W_+ component the value of t_{\min} (14) is relatively large. E.g., for $\sqrt{s_{\text{NN}}} = 2.76$ TeV and $y = 3$ we have $1/t_{\min} \sim (9 \text{ fm})^2$, while for Pb-Pb we need a large impact parameter $b_t > 2R_A \sim 12$ fm in order not to destroy the nuclei (of radius R_A). Therefore, for exclusive J/ψ production in heavy ion collisions, the effective γN energy is not that large and comparable to the γp energies at HERA. Thus, with J/ψ photoproduction in ultra-peripheral Pb-Pb collisions at $\sqrt{s_{\text{NN}}} = 2.76$ TeV [18], we may study the nuclear modification effects on the gluon PDF but not so much its behaviour at very low x .

In the case of Pb- p collisions the dominant contribution comes from the amplitude where the Pb emits the photon. For Pb, the photon flux in the cross section has a strong Z^2 enhancement, not noticeably suppressed by the steep Pb form factor as the main contribution comes from very small q_T^2 . Conversely, due to strong screening effects and a form factor suppression, the cross section from two gluon exchange grows at large A only $\sim A^{2/3}$. As a consequence, studies of Pb- p (or p -Pb) collisions could provide data with a much suppressed W_- contribution, leading to a more direct extraction of the small x gluon. At LHCb, the different beam orientations of Pb- p and p -Pb will effectively provide a probe of the W_+ and the W_- contributions, respectively.

4 Combined description of HERA and LHCb J/ψ data

Our analysis includes not only the HERA photoproduction data but also electroproduction data at larger values of \bar{Q}^2 . Therefore we have to take into account the scale dependence of the gluon PDF. Besides, we need the scale dependence in order to compute the unintegrated gluon distribution, f , of Eq. (9). At leading order (LO), it is sufficient to use a simple parametric form

$$xg(x, \mu^2) = Nx^{-\lambda} \quad \text{with } \lambda = a + b \ln(\mu^2/0.45 \text{ GeV}^2), \quad (16)$$

where the free parameters N , a and b are determined by a non-linear χ^2 fit to the exclusive J/ψ data from HERA and LHCb.

However, at NLO we have to account for the effect of the running of α_s in the DGLAP evolution. In the leading log approximation this leads to a slower growth of the power. Thus in the NLO case we use a parametrisation which explicitly includes the double logarithmic factor $\exp[\sqrt{16N_c/\beta_0} \ln(1/x) \ln(G)]$ coming from the summation of the leading $(\alpha_s \ln(1/x) \ln \mu^2)^n$ contributions. In Eq. (17) below we use the one-loop α_s coupling and allow for the single log contribution via the free parameters: the variable a to account for the x -dependence and the variable b to account for the μ -dependence,

$$xg(x, \mu^2) = Nx^{-a}(\mu^2)^b \exp\left[\sqrt{16N_c/\beta_0} \ln(1/x) \ln(G)\right] \quad \text{with } G = \frac{\ln(\mu^2/\Lambda_{\text{QCD}}^2)}{\ln(Q_0^2/\Lambda_{\text{QCD}}^2)}. \quad (17)$$

With three light quarks ($N_f = 3$) and $N_c = 3$ we have $\beta_0 = 9$. We take $\Lambda_{\text{QCD}} = 200 \text{ MeV}$ and $Q_0^2 = 1 \text{ GeV}^2$.

Besides the HERA data, we include in the fit the recent LHCb measurements of $d\sigma(pp \rightarrow p + J/\psi + p)/dy$, and account for absorption as described in the previous section.

As discussed in Section 3, there are two amplitudes to produce a J/ψ at a rapidity y with energies squared $W_{\pm}^2 = M_{J/\psi} \sqrt{s} e^{\pm|y|}$, where the two solutions correspond to the diagrams of Fig. 2(a) and (b), and hence our theory prediction is given by

$$\frac{d\sigma^{\text{th}}(pp)}{dy} = S^2(W_+) \left(k_+ \frac{dn}{dk_+}\right) \sigma_+^{\text{th}}(\gamma p) + S^2(W_-) \left(k_- \frac{dn}{dk_-}\right) \sigma_-^{\text{th}}(\gamma p). \quad (18)$$

Here, our theoretical predictions for the cross section $\sigma_{\pm}^{\text{th}}(\gamma p)$ at energies W_{\pm} are weighted by the corresponding absorptive corrections $S^2(W_{\pm})$ of Table 2 and photon fluxes dn/dk_{\pm} for photons of energy $k_{\pm} = x_{\gamma}^{\pm} \sqrt{s}/2 \approx (M_{J/\psi}/2) e^{\pm|y|}$. Due to the small values of W_- the direct fit to the LHCb data depends on our description of J/ψ production at moderate values of the proton momentum fraction x carried by the gluons.

The fluxes dn/dk_{\pm} are calculated by performing the q_T^2 integral in Eq. (13) using F_p from Eq. (15). This is consistent with the fluxes used for the calculation of the survival factors S^2 as described in Section 3. This form of the photon flux is an approximation and typically 5%

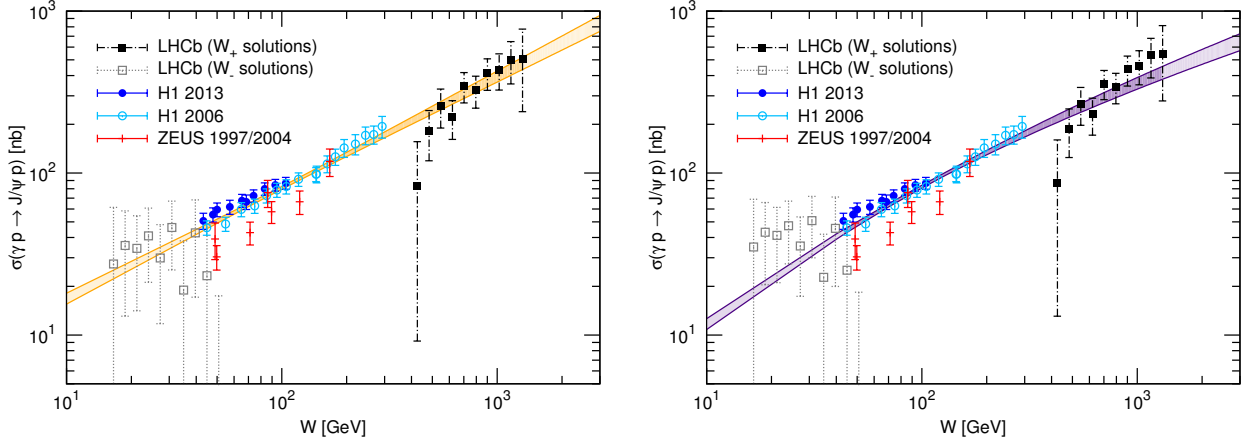


Figure 3: LO (left panel) and NLO (right panel) fits to exclusive J/ψ data. Photoproduction data from H1 [7, 4] and ZEUS [21, 22] are displayed along with the LHCb [5] W_+ and W_- solutions as described in the text. The darker shaded areas indicate the region of the available data. Included in the fit but not displayed are the H1 [7] and ZEUS [22] electroproduction data. The widths of the bands indicate the uncertainties of the fitted cross section resulting from the 1σ experimental error.

smaller than the more precise Equivalent Photon Approximation (EPA) [19].² Our approximation of the photon flux omits terms, proportional to the anomalous magnetic moment of the proton, which contain an additional q_T^2 and, neglecting t_{\min} , these terms have no singularity at $q_T^2 \rightarrow 0$. The corresponding contributions, coming from $q_T \sim 1/R_p$, are concentrated at small b_t and are strongly suppressed by the opacities $\exp[-\Omega_i(s, b_t^2)]$ which are very small ($< 4\%$) in this domain. Note that the flux enters also in the denominator of the survival factors (12) and thus effectively cancels the dependence on the flux in Eq. (18), leaving only the much suppressed dependence in the numerator. We therefore expect the error in $d\sigma^{\text{th}}(pp)/dy$ from the approximation of the photon flux used by us to be much less than 5%.

The results of the combined fit are shown in Fig. 3 for the LO and NLO approaches and the corresponding parameter values are listed in Table 1.³ The fits have $\chi_{\min}^2/\text{d.o.f.}$ a bit larger than 1. This is mainly caused by an inconsistency between the old and the new HERA data as seen in the figures. We emphasise that the ‘effective’ LHCb data points shown in Fig. 3 are not measured directly by the experiment. In the analysis, error bands shown on the cross section are generated using the covariance matrix for the fitted parameters, where, as input, we have added the statistical and systematic experimental errors of the data in quadrature. Hence, the bands correspond to 1σ ‘experimental’ errors. However, there are also ‘theoretical’ errors associated with the model assumptions, the difference between LO and NLO curves gives

²In the LHCb analysis $\sigma(\gamma p)$ is obtained using a simpler formula given in [20] which is about 10% larger than the EPA. However, the measured data for $d\sigma(pp)/dy$ used in our fit do not depend on this.

³Since all the formulae are written just for the low x domain, to be consistent with the previous [3] analysis we neglect HERA data with $x > 0.0055$ in all fits.

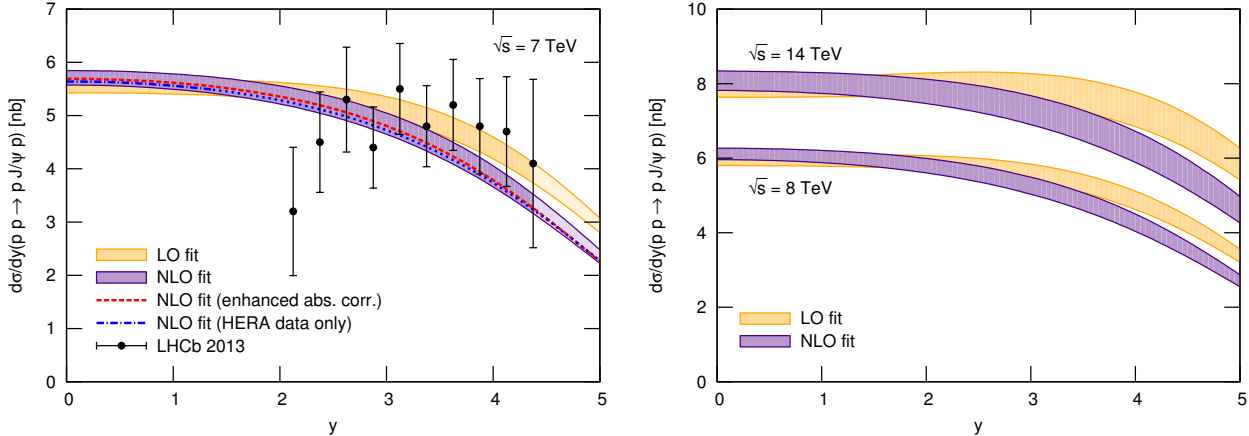


Figure 4: Left panel: LO and NLO fits compared to directly measured LHCb [5] data for $\sqrt{s} = 7$ TeV. Also shown is the NLO fit performed with enhanced absorptive corrections (red dashed line). The NLO fit including only H1 [7, 4] and ZEUS [21, 22] data is also shown (the blue dot-dashed line indicates the range of the HERA data, the blue dotted line indicates the extrapolation to LHCb energies). Right panel: LO and NLO predictions for exclusive J/ψ production at LHCb for $\sqrt{s} = 8$ TeV (lower bands) and $\sqrt{s} = 14$ TeV (upper bands).

	N	a	b	$\chi^2_{\min}/\text{d.o.f.}$
LO	1.27 ± 0.09	0.05 ± 0.01	0.081 ± 0.005	1.13
NLO	0.25 ± 0.04	-0.10 ± 0.01	-0.15 ± 0.06	1.21

Table 1: Values of the three parameters of the LO and NLO gluon fits and corresponding $\chi^2_{\min}/\text{d.o.f.}$

some idea of this error.

In Fig. 4 we compare the LO and NLO fits with the directly measured LHCb data used in our analysis. In this figure we also show the prediction for the LHCb data which would result from an analysis of the HERA data alone. It is clear that, with the current accuracy of the LHCb data, the fit is mainly driven by the HERA data. We also show a prediction for exclusive J/ψ production at the LHCb for $\sqrt{s} = 8$ and 14 TeV. We see that future measurements at the LHC will yield valuable, unique information on the gluon PDF at low scales.

The suppression factor S^2 of Eq. (12) accounts for the probability of additional interactions between the incoming quark-spectators. Besides this, there may be an interaction between the incoming quark/parton in one proton and one of the intermediate partons inside the ladder (the so-called *enhanced* diagrams), which describes the evolution of the low- x gluon. Since these partons have larger transverse momenta, p_T , this probability should be smaller (the absorptive cross section $\sigma^{\text{abs}} \propto 1/p_T^2$). We evaluate the possible ‘enhanced’ effect using again the KMR model [8]. The result is shown by the red dashed line in the left panel of Fig. 4. As seen the role of enhanced absorption is negligible in comparison with the present accuracy of the data.

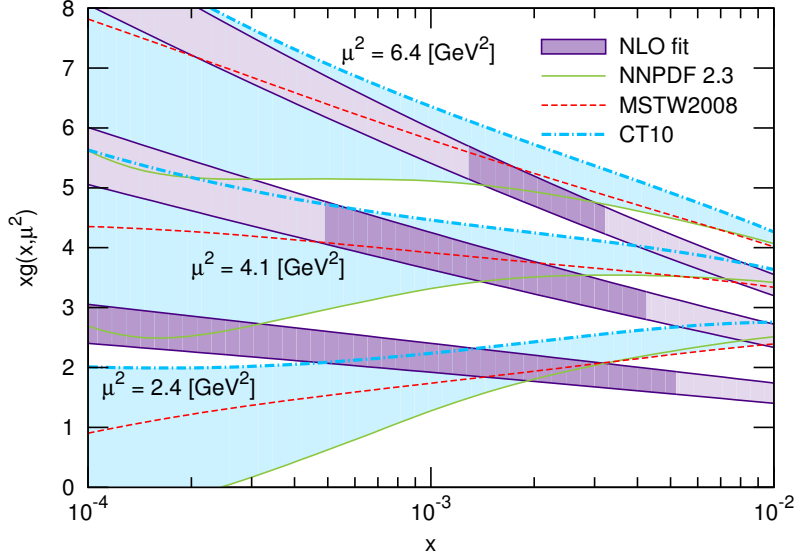


Figure 5: NLO gluon resulting from a fit to all available data evaluated at scales of $\mu^2 = \bar{Q}^2 = 2.4, 4.1$ and 6.4 GeV^2 compared to the global fits NNPDF 2.3 [23], CT10 [24] and MSTW2008 [25]. The dark shading indicates the regions which are directly probed by these data. The pale bands span the range of the central values of the gluon PDFs in three recent global analyses. The actual errors of the individual ‘global’ gluon PDFs are large, particularly below $x = 10^{-3}$.

In Fig. 5 we compare the integrated gluon extracted from our NLO fit to the combined HERA and LHCb exclusive J/ψ data with those given in recent global parton analyses at scales $\mu^2 = \bar{Q}^2 = 2.4, 4.1$ and 6.4 GeV^2 . Note that the LHCb exclusive data actually provide a probe of the gluon down to $x \approx 5.6 \times 10^{-6}$. For such low values of x the present global analyses are unable to determine the gluon PDF. In general, while our NLO gluon fit is lower than the global fits at larger x , it does not show the tendency to fall at small x even at the J/ψ photoproduction scale $\bar{Q}^2 = 2.4 \text{ GeV}^2$. At higher scales it is typically smaller than the CT10 gluon but similar in shape. We do not show the comparison with LO gluons, since it is known that the global analyses have large NLO corrections to the gluon.

5 Exclusive Υ production

We can use our formalism, with $M_{J/\psi}$ replaced by M_Υ , adjusting the electronic branching, Γ_{ee} , and with absorptive corrections now given by Table 3, to calculate exclusive $\Upsilon(1S)$ photoproduction $\sigma(\gamma p \rightarrow \Upsilon p)$. Since the Regge expression for the slope reads $B(W) = B_0 + 4\alpha' \ln(W/M_V)$, with M_V the mass of the vector meson, we also have to reduce the slope (3) by $4\alpha' \ln(M_\Upsilon/M_{J/\psi})$, giving $B(W) = 4.63 + 4 \cdot 0.06 \ln(W/90 \text{ GeV})$ for Υ . Due to the larger mass the gluon is sampled at a larger scale, $\bar{Q}^2 \approx 23 \text{ GeV}^2$. Figure 6 shows the $\Upsilon(1S)$ cross section using our LO and NLO fits to the J/ψ data as discussed above. Also shown are the measurements from H1 [26]

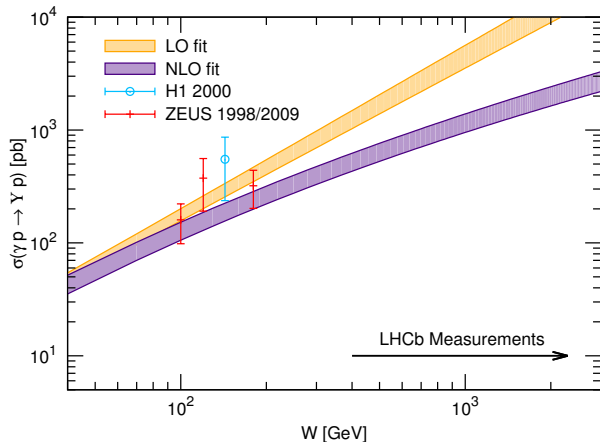


Figure 6: Exclusive $\Upsilon(1S)$ photoproduction prediction resulting from LO and NLO fits to available exclusive J/ψ data from HERA and the LHCb. The H1 [26] and ZEUS [27, 28] measurements are shown for comparison. The arrow indicates the highest energy to which the LHCb experiment is expected to be sensitive with current data (at 7 TeV).

and ZEUS [27, 28]. While both our LO and NLO predictions describe these data reasonably well, the shape of the NLO gluon leads to a much smaller prediction at higher energies. Indeed, due to the double log factor, $\exp[\sqrt{16N_c/\beta_0 \ln(1/x) \ln(G)}]$, the NLO gluon grows with $1/x$ and $\ln(\mu^2)$ less steep than the power-like behaviour, $xg \propto x^{-\lambda}$, of our LO gluon. In turn, once higher energy data become available, this will strongly constrain the shape and scale dependence of the gluon. Data similar to that measured by LHCb for J/ψ photoproduction are expected to become available for Υ shortly.

In Fig. 7 we show our predictions for exclusive $\Upsilon(1S)$ production in pp collisions at LHC energies of 7, 8 and 14 TeV for a rapidity range relevant for LHCb. The large discrepancy between the LO and NLO predictions is a direct consequence of the growing difference between LO and NLO cross sections for increasing W , as seen in Fig. 6. Note that in Fig. 6 we have indicated the highest energies that LHCb is expected to be sensitive to with the current data. It is not surprising that the LO and NLO predictions diverge when extrapolating from the J/ψ region into the unexplored domain of Υ . Figure 7 demonstrates clearly that the expected LHCb data have the potential to strongly constrain the gluon fits.

Note that, due to the steep shape of the imaginary part of the amplitude in the NLO fit for large $x \gtrsim 0.06$ (small W values), the real and skewing corrections are very large. This is more pronounced for the NLO gluon, where the double leading log approximation was adopted in our NLO gluon ansatz (17). However, we must estimate the W_- contributions at small W in order to predict the total measured cross section $d\sigma(pp \rightarrow p + \Upsilon + p)/dy$. On the other hand, for $\Upsilon(1S)$ production, due to the sharply increasing $\sigma(\gamma p)$ cross section, the W_- component typically accounts for less than 15% of the total cross section, so possible uncertainties from these corrections will not change our fits significantly.

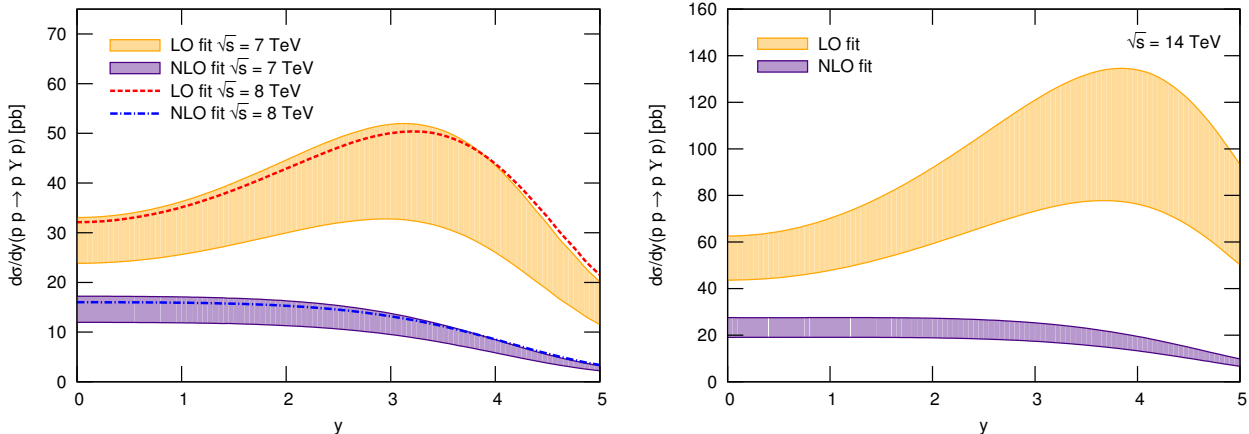


Figure 7: Exclusive $\Upsilon(1S)$ photoproduction prediction resulting from LO and NLO fits to available exclusive J/ψ data from HERA and the LHCb. Left panel: Prediction for LHCb at $\sqrt{s} = 7$ TeV (shaded bands) and at $\sqrt{s} = 8$ TeV (dashed and dot-dashed lines). The uncertainties of the 8 TeV predictions is very similar to the ones shown for 7 TeV. Right panel: Prediction for LHCb at $\sqrt{s} = 14$ TeV.

6 Conclusions

We show that the new HERA data on diffractive J/ψ photo- and electro-production can be described, together with the exclusive LHCb $pp \rightarrow p + J/\psi + p$ data, in the framework of perturbative QCD. We account for the skewed effect of the unintegrated gluon based on the Shuvaev transform and, assuming dominance of the even-signature, include the contribution of the real part of the amplitude via a dispersion relation. In the case of the proton-proton data we calculate the absorptive corrections using a recent model which satisfactorily describes the TOTEM measurement of both the elastic cross section $d\sigma/dt$ and the cross section for the proton to dissociate into a low mass system.

For the LO fit the gluon distribution is parametrised by the power behaviour of Eq. (16). To better fix the factorisation scale we replace the LO expression by the k_T -factorisation formula (11). In this way we account for some kinematical corrections and obtain a gluon distribution which is effectively at NLO level. To be specific we use the parametrisation (17) which accounts explicitly for the resummation of the leading double logarithms. As a result the obtained gluon PDF is smaller at $x \sim 0.01$ than that given by the conventional global analyses but, unlike them, even at the lowest scale $\bar{Q}^2 = 2.4 \text{ GeV}^2$, it does not decrease with decreasing x .

Based on the gluon distribution resulting from our fit we present predictions for exclusive $\Upsilon(1S)$ production at the LHC at $\sqrt{s} = 7, 8$ and 14 TeV and for J/ψ at 8 and 14 TeV. We conclude that future measurements at the LHC have the potential to probe the behaviour of the gluon PDF in an unexplored domain at much smaller x than is currently possible.

Acknowledgements

We thank Lucian Harland-Lang and Ronan McNulty for discussions and helpful remarks on the manuscript. MGR thanks the IPPP at the University of Durham for hospitality. This work was supported by the grant RFBR 11-02-00120-a and by the Federal Program of the Russian State RSGSS-4801.2012.2.

References

- [1] D.Y. Ivanov, A. Schafer, L. Szymanowski and G. Krasnikov, *Eur. Phys. J. C* **34** (2004) 297 [[hep-ph/0401131](#)].
- [2] A.G. Shuvaev, K.J. Golec-Biernat, A.D. Martin and M.G. Ryskin, *Phys. Rev. D* **60** (1999) 014015 [[hep-ph/9902410](#)].
- [3] A.D. Martin, C. Nockles, M.G. Ryskin and T. Teubner, *Phys. Lett. B* **662** (2008) 252 [[arXiv:0709.4406](#) [[hep-ph](#)]].
- [4] C. Alexa *et al.* [H1 Collaboration], [arXiv:1304.5162](#) [[hep-ex](#)].
- [5] R. Aaij *et al.* [LHCb Collaboration], *J. Phys. G* **40** (2013) 045001 [[arXiv:1301.7084](#) [[hep-ex](#)]].
- [6] M.G. Ryskin, *Z. Phys. C* **57** (1993) 89.
- [7] A. Aktas *et al.* [H1 Collaboration], *Eur. Phys. J. C* **46** (2006) 585 [[hep-ex/0510016](#)].
- [8] V.A. Khoze, A.D. Martin and M.G. Ryskin, [arXiv:1306.2149](#) [[hep-ph](#)].
- [9] P. Hoodbhoy, *Phys. Rev. D* **56** (1997) 388 [[hep-ph/9611207](#)].
- [10] A.D. Martin, C. Nockles, M.G. Ryskin, A.G. Shuvaev and T. Teubner, *Eur. Phys. J. C* **63** (2009) 57.
- [11] M.A. Kimber, A.D. Martin and M.G. Ryskin, *Eur. Phys. J. C* **12** (2000) 655 [[hep-ph/9911379](#)].
- [12] G. Watt, A.D. Martin and M.G. Ryskin, *Eur. Phys. J. C* **31** (2003) 73 [[hep-ph/0306169](#)].
- [13] B. Schmidt and M. Steinhauser, *Comput. Phys. Commun.* **183** (2012) 1845 [[arXiv:1201.6149](#) [[hep-ph](#)]].
- [14] A. Bzdak, L. Motyka, L. Szymanowski and J.-R. Cudell, *Phys. Rev. D* **75** (2007) 094023 [[hep-ph/0702134](#)].

- [15] V.A. Khoze, A.D. Martin and M.G. Ryskin, Eur. Phys. J. C **24** (2002) 459 [hep-ph/0201301].
- [16] W. Schafer and A. Szczurek, Phys. Rev. D **76** (2007) 094014 [arXiv:0705.2887 [hep-ph]].
- [17] G. Antchev *et al.* [TOTEM Collaboration], Europhys. Lett. **95** (2011) 41001 [arXiv:1110.1385 [hep-ex]]; *ibid.* **96** (2011) 21002 [arXiv:1110.1395 [hep-ex]]; *ibid.* **101** (2013) 21002; *ibid.* **101** (2013) 21004.
- [18] B. Abelev *et al.* [ALICE Collaboration], Phys. Lett. B **718** (2013) 1273 [arXiv:1209.3715 [nucl-ex]].
- [19] V.M. Budnev, I.F. Ginzburg, G.V. Meledin and V.G. Serbo, Phys. Rept. **15** (1975) 181.
- [20] M. Drees and D. Zeppenfeld, Phys. Rev. D **39** (1989) 2536.
- [21] J. Breitweg *et al.* [ZEUS Collaboration], Z. Phys. C **75** (1997) 215 [hep-ex/9704013]; Eur. Phys. J. C **6** (1999) 603 [hep-ex/9808020].
- [22] S. Chekanov *et al.* [ZEUS Collaboration], Nucl. Phys. B **695** (2004) 3 [hep-ex/0404008].
- [23] R.D. Ball, V. Bertone, S. Carrazza, C.S. Deans, L. Del Debbio, S. Forte, A. Guffanti and N.P. Hartland *et al.*, Nucl. Phys. B **867** (2013) 244 [arXiv:1207.1303 [hep-ph]].
- [24] H.-L. Lai, M. Guzzi, J. Huston, Z. Li, P.M. Nadolsky, J. Pumplin and C.-P. Yuan, Phys. Rev. D **82** (2010) 074024 [arXiv:1007.2241 [hep-ph]].
- [25] A.D. Martin, W.J. Stirling, R.S. Thorne and G. Watt, Eur. Phys. J. C **63** (2009) 189 [arXiv:0901.0002 [hep-ph]].
- [26] C. Adloff *et al.* [H1 Collaboration], Phys. Lett. B **483** (2000) 23 [hep-ex/0003020].
- [27] J. Breitweg *et al.* [ZEUS Collaboration], Phys. Lett. B **437** (1998) 432 [hep-ex/9807020].
- [28] S. Chekanov *et al.* [ZEUS Collaboration], Phys. Lett. B **680** (2009) 4 [arXiv:0903.4205 [hep-ex]].

y	7 TeV		8 TeV		14 TeV	
	$S^2(W_+)$	$S^2(W_-)$	$S^2(W_+)$	$S^2(W_-)$	$S^2(W_+)$	$S^2(W_-)$
0.125	0.911	0.914	0.912	0.915	0.916	0.919
0.375	0.907	0.918	0.908	0.918	0.912	0.921
0.625	0.903	0.921	0.904	0.921	0.909	0.924
0.875	0.898	0.923	0.899	0.924	0.905	0.926
1.125	0.893	0.926	0.894	0.927	0.901	0.929
1.375	0.887	0.929	0.889	0.929	0.896	0.931
1.625	0.880	0.931	0.883	0.931	0.891	0.933
1.875	0.873	0.933	0.876	0.933	0.885	0.935
2.125	0.865	0.935	0.868	0.935	0.879	0.936
2.375	0.855	0.937	0.859	0.937	0.872	0.938
2.625	0.845	0.938	0.849	0.939	0.864	0.940
2.875	0.832	0.940	0.837	0.940	0.855	0.941
3.125	0.818	0.942	0.824	0.942	0.844	0.943
3.375	0.801	0.943	0.808	0.943	0.833	0.944
3.625	0.781	0.944	0.790	0.945	0.819	0.945
3.875	0.758	0.946	0.768	0.946	0.803	0.946
4.125	0.730	0.947	0.743	0.947	0.785	0.948
4.375	0.697	0.948	0.712	0.948	0.763	0.949
4.625	0.659	0.949	0.677	0.949	0.737	0.950
4.875	0.615	0.950	0.635	0.950	0.707	0.951
5.125	0.566	0.951	0.589	0.951	0.671	0.952
5.375	0.516	0.952	0.538	0.952	0.629	0.953
5.625	0.471	0.953	0.489	0.953	0.582	0.953
5.875	0.443	0.954	0.451	0.954	0.531	0.954

Table 2: Rapidity gap survival factors for exclusive J/ψ production, $pp \rightarrow p + J/\psi + p$ at LHC energies of 7, 8 and 14 TeV calculated within model 4 of [8]. Shown are the squared suppression factors S^2 at the two γp energies W_+ and W_- for a given rapidity y in the range $y = 0$ to 6.

	7 TeV		8 TeV		14 TeV	
y	$S^2(W_+)$	$S^2(W_-)$	$S^2(W_+)$	$S^2(W_-)$	$S^2(W_+)$	$S^2(W_-)$
0.125	0.888	0.894	0.890	0.895	0.897	0.901
0.375	0.882	0.899	0.884	0.900	0.892	0.905
0.625	0.875	0.903	0.878	0.905	0.886	0.909
0.875	0.867	0.907	0.870	0.908	0.880	0.913
1.125	0.858	0.911	0.862	0.912	0.874	0.916
1.375	0.848	0.915	0.852	0.916	0.866	0.919
1.625	0.837	0.918	0.841	0.919	0.858	0.921
1.875	0.823	0.921	0.829	0.921	0.848	0.924
2.125	0.808	0.924	0.814	0.924	0.837	0.926
2.375	0.790	0.926	0.797	0.927	0.824	0.929
2.625	0.768	0.928	0.778	0.929	0.810	0.931
2.875	0.743	0.931	0.754	0.931	0.793	0.933
3.125	0.713	0.933	0.726	0.933	0.773	0.934
3.375	0.677	0.935	0.694	0.935	0.749	0.936
3.625	0.636	0.936	0.655	0.937	0.721	0.938
3.875	0.590	0.938	0.611	0.938	0.688	0.939
4.125	0.540	0.940	0.562	0.940	0.650	0.941
4.375	0.491	0.941	0.512	0.942	0.605	0.942
4.625	0.451	0.943	0.466	0.943	0.556	0.944
4.875	0.435	0.944	0.436	0.944	0.504	0.945
5.125	0.452	0.945	0.435	0.946	0.456	0.946
5.375	0.502	0.947	0.469	0.947	0.423	0.947
5.625	0.570	0.948	0.531	0.948	0.417	0.948
5.875	0.652	0.949	0.604	0.949	0.448	0.949

Table 3: Rapidity gap survival factors for exclusive $\Upsilon(1S)$ production, $pp \rightarrow p + \Upsilon + p$ at LHC energies of 7, 8 and 14 TeV, calculated within model 4 of [8].